Journal of Materials Chemistry A

Highly stable electrocatalysts supported on nitrogen-self-doped three-dimensional graphene-like networks with hierarchical porous structure

Journal:	*Journal of Materials Chemistry A*
Manuscript ID:	TA-ART-10-2014-005552.R1
Article Type:	Paper
Date Submitted by the Author:	28-Oct-2014
Complete List of Authors:	Cheng, Juhong; Sun Yat-sen University, Li, Yunyong; Sun Yat-Sen University, Huang, Xiangdong; Guangzhou Automobile Group Co., Ltd, Wang, Qingquan; Guangzhou Automobile Group Co., Ltd, Mei, Ao; Guangzhou Automobile Group Co., Ltd, Shen, Pei; Sun Yat-sen University,

Graphical Abstract

Pt nanoparticles anchored on the nitrogen-self-doped three-dimensional graphene-like networks (Pt/N-3D GNs) exhibits enhanced ORR performance and highly stable.

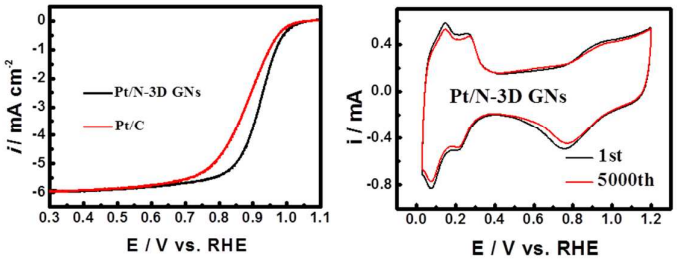

Journal of
Materials Chemistry A

Cite this: DOI: 10.1039/c0xx00000x

ARTICLE TYPE

www.rsc.org/xxxxxx

Highly stable electrocatalysts supported on nitrogen-self-doped three-dimensional graphene-like networks with hierarchical porous structure

Juhong Cheng,[a] Yunyong Li,[a] Xiangdong Huang,*[b] Qingquan Wang,[b] Ao Mei,[b] Pei Kang Shen,*[a]

Received (in XXX, XXX) Xth XXXXXXXXX 20XX, Accepted Xth XXXXXXXXX 20XX
DOI: 10.1039/b000000x

The nitrogen-self-doped three-dimensional graphene-like networks (N-3D GNs) with suitable surface area and hierarchical porous structure have been synthesized by an improved ion-exchange/activation method. The Pt nanoparticles supported on N-3D GNs gives more than double mass activity and almost no degradation in surface area after 5,000 cycles compared with commercial Pt/C catalyst. The results demonstrate that the improvement in the support can reach 2.6 times of the catalytic activity. This strategy is a direct way to reduce the catalyst cost and make the catalyst for practical application reality.

1. Introduction

Fuel cells have been intensively studied due to their better energy conversion efficiency and high power density in per volume [1]. But, the reduction of the Pt usage is a critical challenge for the commercialization of fuel cell vehicles because of its high cost and limited resource availability [2]. In order to reduce the amount of Pt metal used, Pt is usually dispersed on carbon support to improve its utilization. The main requirements of the suitable supports for fuel cell catalysts including high surface area, good electrical conductivity, suitable porosity to allow good mass transport of the reactants and by-products, and high stability in fuel cell environment [3]. The reason why the carbon like Vulcan XC-72 carbon is most widely used as support is due to its high availability and low cost. However, these carbon supports are not highly stable with limited surface area. As a critical problem in electrochemistry, the conductivity of the carbon is required to be improved through a graphitization. That is why considerable efforts have been devoted to develop new carbon materials with special physicochemical properties to improve both catalytic activity and stability [4-7].

The emergence of graphene has attracted great attention in various applications as energy storage materials, polymer composites and mechanical resonators [8-12]. The specific surface area of a single graphene sheet is over 2600 $m^2 g^{-1}$, which makes it desirable for use as a 2-D catalyst support [13]. In spite of the high surface area and superior conductivity, graphene as a support for large-scale application still remains great challenges. The major problem is that graphene is easily agglomeration due to interaction between individual layers, especially to make powder samples, which are unsuitable for the dispersion of precious metal particles [13, 14]. Synthesis of a three-dimensional graphene architecture may secure the applicability of graphene as electrode material according to suppressing its aggregation. Moreover, doping with heteroatoms, such as B, N or S, can also be applied to further tailor the catalytic support properties of graphene[15-17]. In particularly, nitrogen doping is well-known to modify the electronic properties of graphene. So far, several experimental techniques have been developed to make N-doped graphene, including arc charge method [18], the chemical vapor deposition (CVD) with methane and ammonia [19, 20], and plasma method [21]. However these methods are either high cost or difficult for large scale preparation.

Herein, we report a cheap ion-exchange/activation combination method for large scale preparation of the nitrogen-self-doped three-dimensional graphene-like networks (N-3D GNs) as catalyst support for fuel cell application. The novel structure provides multi-dimensional inter-connected pores that facilitate the diffusion of the reactants and by-products. The high specific surface area enables the preparation of highly dispersed metal particles and graphene-like structure, resulting in excellent electronic conductivity. While the doped nitrogen can change the growth behavior of the subsequently deposited catalyst particles, resulting in catalyst-support interactions to increase the activity and durability of Pt catalyst [22]. As a catalyst for oxygen reduction reaction (ORR), the Pt/N-3D GNs showed an enhanced performance in terms of mass activity and stability compared with that of commercial Pt/C catalyst. The better ORR performance of the Pt/N-3D GNs catalysts shows their potential applications in polymer electrolyte membrane fuel cells.

2. Experimental

2.1. Synthesis of support and catalysts

The N-3D GNs were prepared by an improved method that is similar to our early report [23]. Typically, the pretreated macroporous acrylic type anion-exchange resin (D314, Sunresin New Materials Co. Ltd., China) was firstly impregnated with 0.05 mol L^{-1} of sodium cobaltinitrite solution (100 mL). The cobalt ion exchanged resin was washed and dried. Then, the cobalt ion exchanged resin (10 g) was added into 400 mL KOH/ethanol solution containing 15 g KOH under stirring and dried to form cobalt ion exchanged resin/KOH mixture. Finally, the mixture was heated at 850 ^{o}C for 2 h in N_2 atmosphere with a heating rate of 2 ^{o}C min^{-1}. After cooling down to room temperature, the resulting sample was treated with 3 mol L^{-1} HCl solutions to remove cobalt particles and other impurities. Afterwards, the N-3D GNs was repeatedly washed by deionized water and then dried at 120 ^{o}C for 5 h.

The nitrogen-free three-dimensional graphene-like networks (denoted as 3D GNs) is similar with that of N-3D GNs except the resin was replaced by macroporous acrylic type cation-exchange resin (D113) and the exchanged solution was cobalt nitrate. In our work, the macroporous acrylic type anion-exchange resin D314 was used as carbon source for N-3D GNs because of its amino groups. After annealing in the tube furnace, N was self-doped in the products.

In addition, the heat treatment of D113 resin at 850 ^{o}C for 2 h in N_2 (denoted as C-Pristine) but without ion-exchange and KOH activation process was conducted for comparison.

Pt deposition on obtained N-3D GNs (or 3D GNs and C-Pristine) were prepared by the intermittent microwave heating (IMH) method [24]. The weight percentage of Pt in Pt/N-3D GNs, Pt/3D GNs and Pt/C-Pristine electrocatalysts identified by the ICP-OES was 40.1 wt%, 42.6 wt%, and 38.7%, respectively. The commercial Pt/C (46.7 %Pt, TKK, Japan) was used for comparison. (more details in synthesis of 3D GNs, C-Pristine, and catalysts can be seen in supporting information).

2.2. Physical characterization

The X-ray diffraction (XRD) measurements were carried out on a D/Max-III (Rigaku Co., Japan) using CuKα radiation with a scan rate of 10^{o} min^{-1}. Raman spectrometer (Renishaw Corp., UK) using a He–Ne laser with a wavelength of 633 nm was adopted for measurements. The transmission electron microscopic (TEM) investigation was carried out on a JEOL JEM-2010 (HR) at 200 kV. Scanning electron microscopic (SEM) micrograms were collected on a JEM-6700F field emission scanning electron microscope. The X-ray photoelectron spectroscopy (XPS) measurements were carried out on an XPS apparatus (ESCALAB 250, Thermo-VG Scientific Ltd.). The N_2 adsorption experiments using an ASAP 2420 Surface Area Analyzer (Micrometeritics Co., USA) were conducted to investigate the porosity of the samples. Power conductivity under different pressure was examined by four-probe method.

2.3.Electrochemical characterization

The ORR tests were carried out on a bipotentiostat (AFCBP1E, Pine Instrument Co., USA) in a thermostat-controlled standard three-electrode cell in an oxygen-saturated 0.1 mol L^{-1} $HClO_4$ solution scanned between 0 to 1.2 V (*vs.* RHE) at a scan rate of 5 mV s^{-1}. A platinum foil and a reversible hydrogen electrode (RHE) were used as counter and reference electrodes, respectively. A certain amount of electrocatalysts were dispersed in 1.95 mL ethanol and a 0.5 mL 0.5 wt% Nafion suspension (DuPont, USA) under ultrasonic agitation to form a well-dispersed ink with a platinum concentration of 1 mg/ml. Then, 10 μL of the ink was deposited onto the rotating ring-disk electrode. The accelerated durability test (ADT) was achieved by continuous potentiodynamic sweeping carried out between 0.6 and 1.1 V (*vs.* RHE) with a scan rate of 100 mV s^{-1} in oxygen-saturated $HClO_4$ solution.

3. Results and discussion

Fig. 1a shows the XRD patterns of C-Pristine, 3D GNs and N-3D GNs. The sharp diffraction intensity of peak at 26.3° for 3D GNs and N-3D GNs was assigned to graphite (002) peak, suggesting a high degree of graphitization was achieved after exchange with Co ions. While, for C-Pristine with no Co ions exchange, it only gives a broad peak, implying no distinct graphitization. High degree of graphitization means good electrical conductivity for providing electrical pathways, which is an essential condition as catalyst support. The conductivity under 8 MPa for N-3D GNs, 3D GNs and C-Pristine were 793, 877, and 113 S m^{-1} respectively (Table S1). The results are in accordance with XRD data. Fig.1b shows the Raman spectra of three kinds of supports. The band observed at 1351 cm^{-1} is the D-band that attributed to the vibrations of carbon atoms with dangling bonds in disordered graphite planes and the defects incorporated into pentagon and heptagon graphite-like structures. The G-band at 1584 cm^{-1} is corresponding to a splitting of the E2g stretching mode of graphite and reflects the structural intensity of the sp^2-hybridized carbon atom [24]. The degree of graphitization can be calculated from the relative intensities of the D and G bands in the Raman spectrum. The intensity ratio of G-band to D-band (I_G/I_D) for N-3D GNs and 3D GNs were 1.90 and 1.93, respectively, suggesting an extremely high degree of graphitization. By contrast, the I_G/I_D for C-Pristine was just 1.1, which is in good aggrement with the XRD results.

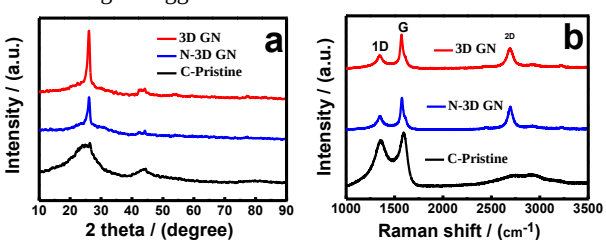

Fig.1. XRD patterns (a) and Raman spectra (b) of C-Pristine, 3D GNs and N-3D GNs.

Fig. 2a shows the nitrogen adsorption/desorption isotherm of C-Pristine, 3D GNs, N-3D GNs and Pt/N-3D GNs.samples. The C-Pristine sample made for comparison by heat treatment of D113 resin directly gave the Brunauer–Emmett–Teller (BET) surface area of 137.8 m^2 g^{-1}. For 3D GNs and N-3D GNs, the isotherms showed combined characteristics of type II

and type IV isotherms with high specific surface area of 729 and 745 $cm^2 g^{-1}$, repectively. As we known, the considerable high specific surface area of the support could provide high dispersion of the active components, but such an ultrahigh surface area of 1810 $m^2 g^{-1}$ reported in literature [23] may make it very vulnerable to electrochemical corrision [25]. In this work, the specific surface areas of 3D GNs and N-3D GNs were reduced to a value range that aimed at ensuring the dispersion and stability by adjusting the amount of KOH added in the synthesis process. The surface area of Pt/N-3D GNs can be reached at 500 $m^2 g^{-1}$.

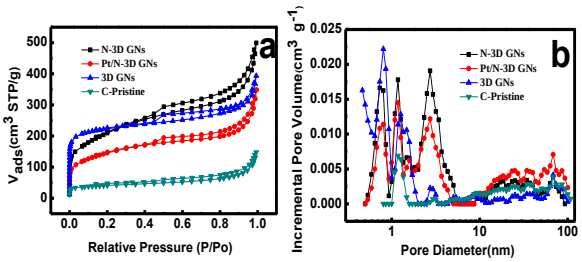

Fig.2.Nitrogen adsorption/desorption isotherms (a) and DFT pore-size distribution curves (b) of C-Pristine, 3D GNs, N-3D GNs and Pt/N-3D GNs.

The pore size distribution (Fig.2b) was determined by the DFT method. All of the samples investigated show a pore size distribution with a micro-, meso-, and macro- hierarchical pore structure. The pores ranged from micro- to macro-size are not only in favor of good dispersion[26], but also benefited for effective diffusion of the reactants and by-products. From the surface area and pore structure data in Table S2, It can be seen that the Pt/N-3D GNs have a slightly pore structure change in terms of the total volume of pores at P/P0=0.98 and proportion t-Plot micropore volume, suggesting that depositing Pt nanoparticles didn't damage the thee dimensional hierarchical pore structure of the support. Assuming that Pt do not change the surface area, Pt/N-3D GNs calculated by carbon only has very similar surface area (731 $cm^2 g^{-1}$) and volume of pore with those of N-3D GNs (Fig.S1). This means that most of the Pt nanoparticles were located at the surface of the support, and very little particles was inserted into the pores. In that case, reactants can effectively diffuse onto the surface of catalysts through the interconnected porous channels and in further enhance the catalytic performance.

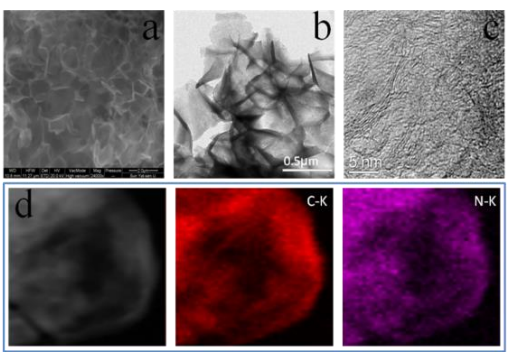

Fig.3. SEM (a), TEM(b) and high-resolution TEM(c) images of the N-3D GNs sample; (d) HAADF image and corresponding mapping images of one pore in the N-3D GNs sample.

The morphologies of the N-3D GNs samples were characterized by scanning electron microscopy (SEM) and transmission electron microscopy (TEM). Fig. 3a and b show the interconnected 3D porous network of the support. The interconnected N-3D GNs exhibited sub-micrometer-sized pores and graphene-like thin layer walls. Moreover, the lattice fringes of graphene in the high-resolution TEM image (Fig. 3c) confirmed the graphitization of the N-3D GNs materials, which is consistent with that of XRD and Raman results. The crystallinity of the graphene wall also showed a certain degree of curvature because of the activation by KOH. Fig. 3d is the TEM mapping images of one pore in the N-3D GNs sample, which indicates that N was homogeneously doped in the graphene-like network.

The Pt nanoparticles were loaded on three types of support materials by chemical adsorption/reduction processes to form nanocomposites. Fig. 4 shows the TEM images (a, b, c) and corresponding size-distribution histograms (c, d, e) of Pt/C-Pristine, Pt/3D GNs and Pt/N-3D GNs samples, respectively. It can be found that the Pt particles deposited on C-Pristine samples appeared aggregation, while, Pt nanoparticles distributed on the 3D GNs and N-3D GNs samples were quite uniform. According to the size distributions obtained by measuring the sizes of 100 randomly selected particles, the average Pt particle sizes were 5.7, 3.4 and 3.0 nm for Pt/C-Pristine, Pt/3D GNs and Pt/N-3D GNs, respectively. The reason for big Pt nanoparticles of $Pt/C_{Pristine}$ is its high Pt loading but low surface area of $C_{Pristine}$. Compared with Pt/3D GNs, Pt/3D GNs have slightly narrower and smaller Pt nanoparticles. This is ascribed to the increased number of nucleaton sites provided by the addtion of the nitrogen functionalities into the three dimensional graphene networks [27, 28].

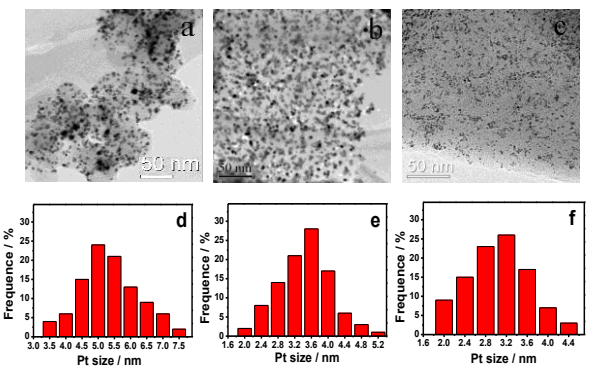

Fig.4. TEM images of (a) Pt/C-Pristine, (b) Pt/3D GNs and (c) Pt/N-3D GNs. Particle size histograms of (d) Pt/C-Pristine, (e) Pt/3D GNs and (f) Pt/N-3D GNs.

N-doping was confirmed in the XPS of the N-3D GNs sample (Fig.S2), which is consistent with the TEM result in Fig. 3d. Fig. 5b shows the N 1s XPS spectra of Pt/N-3D GNs which could be reasonablely deconvoluted into three kinds of nitrogen functional groups: pyridinic-type N (398.5 eV), pyrrole-type N (400.2 eV) and graphitic-type N (401.1 eV) [29].

The elemental analysis results show that the N concentration was 1.9 at% for Pt/N-3D GNs, while N is hardly detectable for the Pt/C-Pristine and Pt/3D GNs samples. Fig.5b shows the XPS-Pt4f spectra of Pt/N-3D GNs, Pt/3D GNs and Pt/C-Pristine. The Pt 4f binding energy of Pt/N-3D GNs has a negative shift compared with those of Pt/3D GNs and Pt/C-Pristine. The shift is induced by the proposed occurrence of electron-donation from nitrogen defects to Pt in N-doped systems [30-32].

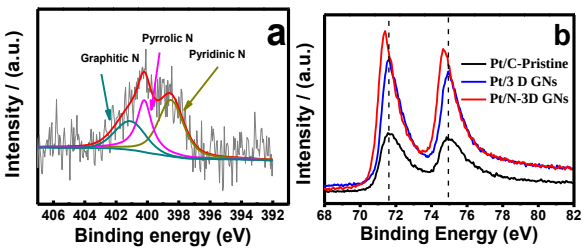

Fig.5. (a) XPS core level spectra of Pt/N-3D GNs N1s, (b) XPS-Pt4f spectra of the Pt/N-3D GNs, Pt/3D GNs and Pt/C-Pristine

The core level spectra of C1s and Pt4f of the Pt/C-Pristine, Pt/3D GNs and Pt/N-3D GNs are shown in Fig.S3. For Pt/C-Pristine and Pt/3D GNs samples, the C1s spectra exhibited a certain degree of oxidation and could be deconvoluted into three different chemical environments: C–C (284.6 eV), C–O (286.5 eV), and O=C-O (289.1 eV). Comparatively, the C1s of Pt/N-3D GNs exhibited an additional band at 285.6 eV which corresponding to C–N [27].

The oxidation states of Pt in the three samples are also determined, and the principle peaks can be attributed to similar four components: $Pt^0(4f_{7/2})$ at 71.6 eV, Pt^{2+} at 72.4 eV, $Pt^0(4f_{5/2})$ at 74.8 eV and Pt^{2+} at 76 eV [33]. The results of the fitted peak positions and compositions obtained from the XPS analysis are summarized in Table S3. Compared to Pt/3D GNs, the Pt/N-3D GNs have a higher level of Pt^0 component. This finding is consistent with the previous study of Pt/N-modified carbon catalysts and is consistent with the occurrence of electron-donation from nitrogen defects to Pt in N-doped systems[34].

The electrocatalytic behavior of Pt/C-Pristine, Pt/3D GNs, Pt/N-3D GNs and the Pt/C (TKK 46.7%) as the benchmark towards ORR were examined by the rotating ring-disk electrode (RRDE) polarization curves in oxygen-saturated 0.1 mol L^{-1} $HClO_4$ at 25 ^oC with a scan rate of 5 mV s^{-1}. As shown in Fig.6a, Pt/C-Pristine has the lowest catalytic activity in terms of onset potential and half-wave potential, which is caused by the low conductivity of C-Pristine, poor dispersion of Pt nanoparticles and weak interaction between catalyst and support. While, the Pt/3D GNs have a more positive half-wave potential in comparison with that of Pt/C. The improved catalytic activity is attributed to the conductivity and structural advantage of N-3D GNs. Firstly, the inter-connected three network structure provides continuous electronic channels. Secondly, the hierarchical pores offers electrochemical reaction three-phase boundary (TPB). Finally, the porosity of N-3D GNs can also facilitate the diffusion of the reactants and by-products within the catalyst layer which enhances the utilization of Pt[35]. The Pt/N-3D GNs sample exhibited the most positive onset potential and its half-wave potential have 20 mV positive shift compared with that of Pt/3D GNs. The further imrovement in activity can be explained by synergistic effect: electon donation (confirmed by XPS results) from N-3D GNs to uncompletely occupied orbital of Pt nanoparticles can increase surface electron density of Pt, which reduces the oxygen adsorption barriers and enhance the activity of oxygen reduction [36].

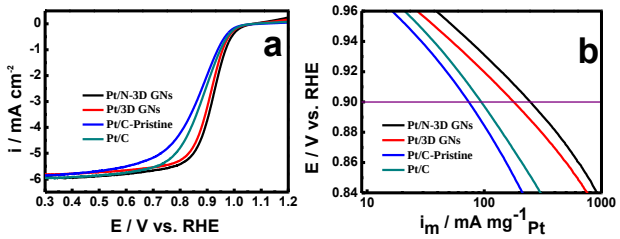

Fig.6. (a) Polarization curves of Pt/N-3D GNs, Pt/3D GNs, Pt/C-Pristine and Pt/C for ORR on RRDE at 1600 rpm in oxygen-saturated 0.1 mol L-1$HClO_4$ at 25 ^oC with a scan rate of 5 mV s^{-1} and (b) Pt-mass activities for ORR on the four different electrocatalysts.

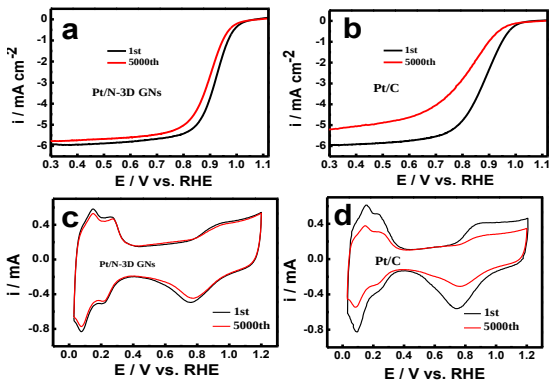

Fig.7. ORR curves of Pt/N-3D GNs (a) and Pt/C (b) before and after accelerated durability test. Cyclic voltammograms in background solution of Pt/N-3D GNs (c) and Pt/C (d) before and after accelerated durability test.

Fig. 6b compares the mass activities of the four different samples at 0.9 V (*vs.* RHE) calculated from the experimental data using the well-known mass transport correction for a rotating disk electrode [29]:

$$i_k = i_d.i / (i_d - i) \quad (1)$$

where i is the experimentally obtained current, i_d refers to the measured diffusion-limited current and i_k the mass-transport-free kinetic current. The measured mass activity of 94.8 mA mg^{-1} on commercial Pt/C catalyst is in good agreement with the reported values in literature [37]. The mass activity of Pt/N-3D GNs measured from the curve in Fig. 6b was 248 mA mg^{-1}, which is 3.4, 2.6, and 1.4 times higher than that of Pt/C-Pristine, Pt/C, and Pt/3D GNs, respectively. The bigger Pt nanoparticle size and agglomeration of $Pt/C_{Pristine}$ (confirmed by the TEM image) might result in a lower specific surface area and therefore less activity sites for oxygen

reduction reaction per unit mass of Pt[27]. The after activated 3D GNs improve the distribution of Pt nanoparticles obviously, the catalytic performance was enhanced greatly. While, for the Pt/N-3D GNs, in addtion to good dispersion and small size effect of Pt nanoparticles, the synergistic effect existed between the N-3D GNs support and Pt which may be responsible for the further improvement in activity.

The stability is one of the critical factors for fuel cell catalysts. In this study, comparisons of the ORR polarization curves and the corresponding cyclic voltammograms (CVs) for Pt/N-3D GNs and Pt/C before and after 5,000 cycles were carried out to evaluate the stability of the Pt/N-3D GNs catalyst. As shown in Fig. 7a and c, the half-wave potential of the Pt/N-3D GNs was 25 mV degradation and almost no change in active surface area after 5,000 cycles. However, there was 93 mV degradation of the half-wave potential and 35 % loss of the active surface area on Pt/C after the same accelerated durability test (Fig. 7b and d). On the one hand, N-doped carbon materials themselves show much better stability and tolerance to crossover effect compared to commercial Pt/C catalyst[38]. Moreover, Pt nanoparticles deposited on N-3D GNs have strong interaction with the support, which can fix Pt nanoparticles well and alleviate the dissolution and reunion of Pt nanoparticles during continuous cycle scanning. Combing the perfect structure and N-doped advantage, a much enhanced activity and improved stability for oxygen reduction is achieved.

4. Conclusions

Using cheap macroporous acrylic type anion-exchange resin as precursor, we have synthesized nitrogen-self-doped three-dimensional grapheme-like network (N-3D GNs) suitable for catalyst support on a large scale. The N-3D GNs have high surface area, good electrical conductivity, perfect pore structure, and N-doping advantage. After anchoring Pt nanoparticles on the stable and highly conductive nitrogen-containing three-dimensional porous graphene-like networks, the Pt/N-3D GNs showed a much better ORR performance and durability than that of the Pt/C catalyst. The results demonstrated that the improvement in the support can reach 2.6 times in the catalytic activity. Combining structure advantage and N-doping effect, the application of N-3D GNs in catalyst support is a promising way to reduce the catalyst cost and make the catalyst for practical application reality.

Acknowledgements

This work was supported by the Specialized Research Fund for the Doctoral Program of Higher Education of China (20110171110024), the Major International (Regional) Joint Research Project (51210002), the Link Project of the National Natural Science Foundation of China and Guangdong Province (U1034003), the National Basic Research Program of China (2015CB932304) and Guangzhou Automobile Group Project (XW6).

Notes and references

[a] *State Key Lab oratory of Optoelectronic Materials and Technologies, School of Physics and Engineering, Sun Yat-sen University, 135 Xingang Road, Guangzhou,510275, PR China. E-mail : stssp k@mail.sysu .edu.cn; Fax: +86-20-84036736; Tel:+86-20-84036736*
[b] *Automotive Engineering Institute, Guangzhou Automobile Group Co., Ltd, Guangzhou, 510640, PR China. E-mail : huangxd@gaei.cn*
[a] *The author contributed equally.*

† Electronic Supplementary Information (ESI) available: [details of any supplementary information available should be included here]. See DOI: 10.1039/b000000x/

1. A. Marinkas, F. Arena, J. Mitzel, G. M. Prinz, A. Heinzel, V. Peinecke and H. Natter, Carbon, 2013, 58, 139.
2. X. Ma, H. Meng, M. Cai and P. K. Shen, Journal of the American Chemical Society, 2012, 134, 1954.
3. E. Antolini, Applied Catalysis B: Environmental, 2009, 88, 1.
4. J.-S. Zheng, X.-S. Zhang, P. Li, X.-G. Zhou and W.-K. Yuan, Catalysis Today, 2008, 131, 270.
5. W. Zhang, P. Sherrell, A. I. Minett, J. M. Razal and J. Chen, Energy & Environmental Science, 2010, 3, 1286.
6. P. V. Shanahan, L. Xu, C. Liang, M. Waje, S. Dai and Y. Yan, Journal of Power Sources, 2008, 185, 423.
7. N. Cheng, S. Mu, X. Chen, H. Lv, M. Pan and P. P. Edwards, Electrochimica Acta, 2011, 56, 2154.
8. S. Stankovich, D. A. Dikin, G. H. Dommett, K. M. Kohlhaas, E. J. Zimney, E. A. Stach, R. D. Piner, S. T. Nguyen and R. S. Ruoff, Nature, 2006, 442, 282.
9. M. D. Stoller, S. Park, Y. Zhu, J. An and R. S. Ruoff, Nano letters, 2008, 8, 3498.
10. E. Yoo, J. Kim, E. Hosono, H.-s. Zhou, T. Kudo and I. Honma, Nano letters, 2008, 8, 2277.
11. B. Seger and P. V. Kamat, The Journal of Physical Chemistry C, 2009, 113, 7990.
12. A. Eichler, J. Moser, J. Chaste, M. Zdrojek, I. Wilson-Rae and A. Bachtold, Nature nanotechnology, 2011, 6, 339.
13. P. V. Kamat, The Journal of Physical Chemistry Letters, 2009, 1, 520.
14. J.-Y. Jhan, Y.-W. Huang, C.-H. Hsu, H. Teng, D. Kuo and P.-L. Kuo, Energy, 2013, 53, 282.
15. J. Qiao, L. Xu, L. Ding, L. Zhang, R. Baker, X. Dai and J. Zhang, Applied Catalysis B: Environmental, 2012, 125, 197.
16. Y. Cheng, C. Xu, P. K. Shen and S. P. Jiang, Applied Catalysis B: Environmental, 2014, 158, 140.
17. J. Zhu and P. K. Shen, RSC Advances, 2013, 3, 14686.
18. L. Panchakarla, K. Subrahmanyam, S. Saha, A. Govindaraj, H. Krishnamurthy, U. Waghmare and C. Rao, Advanced Materials, 2009, 21, 4726.
19. D. Wei, Y. Liu, Y. Wang, H. Zhang, L. Huang and G. Yu, Nano letters, 2009, 9, 1752.
20. L. Qu, Y. Liu, J.-B. Baek and L. Dai, ACS nano, 2010, 4, 1321.
21. Y. Wang, Y. Shao, D. W. Matson, J. Li and Y. Lin, ACS nano, 2010, 4, 1790.
22. M. Groves, A. Chan, C. Malardier-Jugroot and M. Jugroot, Chemical Physics Letters, 2009, 481, 214.
23. Y. Li, Z. Li and P. K. Shen, Advanced Materials, 2013, 25, 2474.
24. C. He, H. Meng, X. Yao and P. K. Shen, International Journal of Hydrogen Energy, 2012, 37, 8154.
25. Y. Takasu, T. Kawaguchi, W. Sugimoto and Y. Murakami, Electrochimica Acta, 2003, 48, 3861.
26. F. Su, J. Zeng, X. Bao, Y. Yu, J. Y. Lee and X. Zhao, Chemistry of materials, 2005, 17, 3960.
27. Y. Zhao, Y. Zhou, R. O'Hayre and Z. Shao, Journal of Physics and Chemistry of Solids, 2013, 74, 1608.
28. S. Stambula, N. Gauquelin, M. Bugnet, S. Gorantla, S. Turner, S. Sun, J. Liu, G. Zhang, X. Sun and G. A. Botton, The Journal of Physical Chemistry C, 2014, 118, 3890.

29. C. He and P. K. Shen, Electrochemistry Communications, 2013, 35, 80.
30. T. Holme, Y. Zhou, R. Pasquarelli and R. O'Hayre, Physical Chemistry Chemical Physics, 2010, 12, 9461.
31. Y. Zhou, K. Neyerlin, T. S. Olson, S. Pylypenko, J. Bult, H. N. Dinh, T. Gennett, Z. Shao and R. O'Hayre, Energy & Environmental Science, 2010, 3, 1437.
32. S. Pylypenko, A. Queen, T. S. Olson, A. Dameron, K. O'Neill, K. Neyerlin, B. Pivovar, H. N. Dinh, D. S. Ginley and T. Gennett, The Journal of Physical Chemistry C, 2011, 115, 13667.
33. Y. Xin, J.-g. Liu, Y. Zhou, W. Liu, J. Gao, Y. Xie, Y. Yin and Z. Zou, Journal of Power Sources, 2011, 196, 1012.
34. B. Xiong, Y. Zhou, Y. Zhao and J. Wang, X. Chen, R. O'Hayre and Z. Shao, Carbon, 2013, 52, 181.
35. T. Maiyalagan, X. Dong, P. Chen and X. Wang, Journal of Materials Chemistry, 2012, 22, 5286.
36. T. Toda, H. Igarashi, H. Uchida and M. Watanabe, Journal of The Electrochemical Society, 1999, 146, 3750.
37. Z. Yan, M. Cai and P. K. Shen, Journal of Materials Chemistry, 2012, 22, 2133.
38. Y. Chen, J. Wang, H. Liu, M. N. Banis, R. Li, X. Sun, T.-K. Sham, S. Ye and S. Knights, The Journal of Physical Chemistry C, 2011, 115, 3769.